Microgravity Sci. Technol. (2014) 26:77–88
DOI 10.1007/s12217-014-9364-2

ORIGINAL ARTICLE

A Novel Microgravity Simulator Applicable for Three-Dimensional Cell Culturing

Simon L. Wuest · Stéphane Richard · Isabelle Walther · Reinhard Furrer · Roland Anderegg · Jörg Sekler · Marcel Egli

Received: 8 July 2013 / Accepted: 26 March 2014 / Published online: 6 June 2014

Abstract Random Positioning Machines (RPM) were introduced decades ago to simulate microgravity. Since then numerous experiments have been carried out to study its influence on biological samples. The machine is valued by the scientific community involved in space relevant topics as an excellent experimental tool to conduct pre-studies, for example, before sending samples into space. We have developed a novel version of the traditional RPM to broaden its operative range. This novel version has now become interesting to researchers who are working in the field of tissue engineering, particularly those interested in alternative methods for three-dimensional (3D) cell culturing. The main modifications concern the cell culture condition and the algorithm that controls the movement of the frames for the nullification of gravity. An incubator was integrated into the inner frame of the RPM allowing precise control over the cell culture environment. Furthermore, several feedthroughs now allow a permanent supply of gas like CO_2. All these modifications substantially improve conditions to culture cells; furthermore, the rewritten software responsible for controlling the movement of the frames enhances the quality of the generated microgravity. Cell culture experiments were carried out with human lymphocytes on the novel RPM model to compare the obtained response to the results gathered on an older well-established RPM as well as to data from space flights. The overall outcome of the tests validates this novel RPM for cell cultivation under simulated microgravity conditions.

Keywords Random Positioning Machine · Microgravity · Tissue engineering · 3D cell cuturing · Kinematic acceleration

Nomenclature

t	Time [s]
I	Inner frame
O	Outer frame
G	Global frame
$\vec{g}_I$(t)	Earth gravitation vector in the inner frame, at the time point t [g]
$\vec{g}_G$	Earth gravitation vector in the global frame [g]
$\alpha(t)$	Rotation angle of the outer frame to the global frame, at the time point t [rad]
α_0	Rotation angle of the outer frame to the global frame, at the time point $t = 0$ [rad]
$\beta(t)$	Rotation angle of the inner frame to the outer frame, at the time point t [rad]
β_0	Rotation angle of the inner frame to the outer frame, at the time point $t = 0$ [rad]
G_{mean}	Mean gravity [g]
$G_{X,mean}$; $G_{Y,mean}$; $G_{Z,mean}$	Mean gravity in X-, Y- and Z-direction (inner frame) [g]
$g_{X,I,i}$, $g_{Y,I,i}$, $g_{Z,I,i}$	Samples indicating the direction of the earth gravity vector transposed to the

S. L. Wuest · R. Anderegg · J. Sekler
Institute for Automation, University of Applied Science Northwestern Switzerland, Windisch, Switzerland

S. L. Wuest · S. Richard · I. Walther · M. Egli (✉)
CC Aerospace Biomedical Science and Technology, Lucerne School of Engineering and Architecture,
Seestrasse 41, 6052 Hergiswil, Switzerland
e-mail: marcel.egli@hslu.ch

R. Furrer
Institute of Mathematics, University of Zurich,
Zürich, Switzerland

inner frame, in the local X-, Y- and Z-directions, respectively [g]

$\vec{p}_{global}(t)$ Arbitrary point in the global frame, at time point t [m]

$\vec{r}_{local}$ Arbitrary point in the local inner frame [m]

$r_{X,local}$, $r_{Y,local}$; $r_{Z,local}$ Coordinates in the X, Y and Z-directions of an arbitrary point $\vec{r}_{local}$ in the local inner frame [m]

r Distance from the center of rotation [m]

ω_α Rotation velocity of the outer frame [rad/s]

ω_β Rotation velocity of the inner frame [rad/s]

ω Rotation velocity if both frames rotate with the same velocity $\omega_\alpha = \omega_\beta = \omega$ [rad/s]

$\vec{A}_{global}(t)$ Acceleration considered in the global frame, at time point t [m/s^2]

$A_{X,global(t)}$, $A_{Y,global}(t)$, $A_{Z,global}(t)$ Acceleration considered in the global frame in X, Y, and Z-direction, respectively, at time point t [m/s^2]

$A_{mean,global}$ Mean acceleration, considered in the global frame [m/s^2]

$\check{A}_{\text{mean,global}}$ Minimum expected mean acceleration [m/s^2]

$\hat{A}_{\text{mean,global}}$ Maximum expected mean acceleration [m/s^2]

$\vec{A}_{local}(t)$ Acceleration in the local inner frame, at time point t [m/s^2]

$A_{mean,local}$ Mean acceleration, considered in the local frame [m/s^2]

Introduction

Regular 2-dimensional (2D) cell culture techniques represent a convenient method to study biological processes. The use of this method has substantially improved our understanding of cellular mechanisms over the last decades. Tissue cells are cultured in plastic dishes, where they anchor to the inner flat surface via the extracellular matrix. Obviously, this conventional 2D approach does not account for the third dimension. Cells naturally belong to a 3-dimensional (3D) organization forming cell clusters or tissues in which mechanical, structural and chemical interactions between cells and/or the extracellular matrix (ECM) take place in all three dimensions.

Indeed, recent evidence reveals striking discrepancies in the behavior of cells cultured in 2D or 3D (Anders et al. 2003; Weaver et al. 1997; Wolf et al. 2003). In fact, 3D cell cultures reflect the *in vivo* situation more accurately than 2D cell cultures, and 3D culture allows reducing the gap between the artificial cell culture *in vitro* and the physiological situation. Therefore, researchers have been looking for 3D cell culture strategies that enable more accurate mimicking of tissue or organ structures and functions. To do so, culture techniques have been constantly developed. Single and co-culture techniques have been developed such as cellular spheroids (Lin and Chang 2008) or polarized epithelial cell culture (Shaw et al. 2004). Spheroidal cell structures for example were introduced in tumor research a long time ago (Santini and Rainaldi 1999; Ivascu and Kubbies 2006; Friedrich et al. 2009).

In that context, spheroids have been shown to better represent characteristics of in vivo tumors. Furthermore, they have also been developed to study angiogenesis (Wenger et al. 2005; Wenger et al. 2004). Of all the strategies to simulate 3D in vivo tissue growth, hydrogels have emerged as an attractive option that provides an artificial environment for optimal 3D cell culture. Such gels consist of collagen (Butcher and Nerem 2004), dextran (Cadee et al. 2000; Cascone et al. 2001), Matrigel™ (Hughes et al. 2010) as well as other materials (Burdick and Prestwich 2011; Eyrich et al. 2007; Ho et al. 2010; Masters et al. 2005). Those gels can be supplemented with particular enzymes and growth factors (Kleinman et al. 1986; Kleinman et al. 1982). In addition to hydrogels, 3D platforms have been developed such as the BioLevitator™ from Hamilton. There, cells loaded with magnetic beads are cultured in 3D while exposed to a magnetic field.

In this paper, an alternative approach to 3D cell culturing by using the RPM is presented. The RPM (van Loon 2007; Borst and Van Loon 2009) is a 3-axis clinostat in which the two axes are essentially rotated at constant speed. Its working concept evolved from simple clinostats, which were developed first in 1879 by Julius von Sachs, a botanist who wanted to investigate gravitropism in plants (van Loon 2007). Through the particular movement generated by the RPM, the weight vector is continually reoriented as in traditional clinorotation, but with directional randomization. The purpose of the original idea was to simulate weightlessness more accurately, but the concept can be applied to generate 3D culture as well. Indeed, randomization of the Earth gravity vector allows redistributing the gravity forces constantly so that cells grow in a similar environment as in organs/tissues (Kraft et al. 2000). Cells cultured under those conditions will no longer sediment, therefore allowing for omnidirectional cell growth. Supporting this idea, a similar approach has already been successfully applied using a rotating wall vessel bioreactor (Barrila et al. 2010). Moreover, it has been recently shown that proliferating endothelial cells cultured on the RPM start to grow as multicellular spheroids. Later on, tubular structures were formed by the spheroidal growing cell structure and a clear increase of extracellular matrix proteins was measured as well (Pietsch et al. 2011).

The evolution of the RPM reported here lies mainly in the full integration of a CO_2 incubator directly on the internal frame of the RPM. Such an upgrade allows

close control of the temperature without the need of a completely air-conditioned room. In addition, CO_2 can constantly be supplied to the cells. CO_2 regulation allows maintaining a constant pH matching physiological conditions (7.2–7.5) and makes additional buffering strategies unnecessary.

Material and Methods

Random Positioning Machine (RPM)

The RPM has a solid lightweight construction that supports two gimbal-mounted frames (Fig. 1). A commercially available CO_2 incubator, slightly modified to fit the needs, is attached to the inner frame, which provides a 14 liter cell culture chamber. The chamber offers optimal culture conditions, such as maintaining defined levels of CO_2 and temperature. In addition, the chamber is equipped with various sensors for monitoring crucial culturing parameters. The movement of the rotating frames is driven by two independently operated and controlled engines via timing belts to avoid slippage. Complicated belt routing is avoided by mounting one engine directly onto the outer frame. This design ensures independent control of the frames movement. The incubator motion is monitored through encoders attached to the motors directly. 3D accelerometers fixed to the inner frame are used for quality control of the movement.

This version of the RPM is equipped with a rotational feed-through for gas and liquids allowing, for example, constant CO_2 supply to the incubator. Power supply for the various devices on the inner and outer frame, as well as time critical communication, are transmitted via slip ring capsules. As an alternative route, non-time critical information can also be transmitted via a WLAN. The WLAN system offers the advantage of being able to monitor crucial RPM data from a nearby office by using a standard web browser. Having the incubator placed in the RPM instead of placing a small (desktop) RPM inside an incubator brings the advantage of a relatively large test chamber. At the same time the confinement of the incubator chamber insures that all samples are in a reasonable distance to the center of rotation in order to avoid centrifugal forces. In addition the incubator does not get contaminated through the RPM machinery such as oil vapor or debris of wear.

The software designed to control the RPM functions is run on a built-in industrial PC and is a LabVIEW based application. Numerous functions have been implemented into the operating software like an automatic start-stop function executable at predefined time/date or the option to monitor all the crucial incubator parameters like temperature, gas composition and motion.

Biological Experiment

All chemicals and drugs used for conducting the mentioned biological experiments were purchased from Sigma (Buchs, Switzerland) unless otherwise stated.

Lymphocytes Culture

Peripheral blood (450 ml) was collected from healthy donors and further processed for lymphocyte isolation as previously described (Cogoli-Greuter et al. 1996; Cogoli-Greuter et al. 1994; Gmunder et al. 1990; Pippia et al. 1996). In brief: a lymphocyte-enriched suspension was prepared by gradient centrifugation using Lymphocyte Separation Medium (PAA, LMS-1077, J15-004). A T lymphocyte enriched suspension was later obtained using a Human T Cell Enrichment kit (RnD research, HTCC-25). The cells were re-suspended in RPMI-1640 supplemented with 40 mM HEPES, 5 mM sodium bicarbonate, gentamycin (50 ∝l/ml), 4 mM L-Glutamine and 10 % fetal calf serum (PAA A15-101). The cells were then transferred into LYCIS containers (1 ml at a density of 1.5 million cells/ml) (Chang et al. 2012) and mounted either at the rotating center of the RPM or in a stationary laboratory incubator (equal incubator as on the RPM). In the experiments described here, the samples that were placed at the rotating center of the RPM (within a radius of 10 cm) experienced a rotation with an angular velocity of 40 deg/s and an ambient temperature of 37 °C. Cells on the RPM were exposed to the RPM simulated microgravity for one hour prior to lymphocyte activation by injection of concanavalin A /CD 28 mixture (10 ∝g/ml and 4 ∝g/ml final concentrations, respectively; performed by a quick interruption of the rotation, $<$ 1 min.). After activation, the cells remained under their respective conditions (simulated microgravity or stationary) for 22 h.

FACS Analysis

For the FACS analysis, T lymphocytes were stained at 4 °C using a CD-25 antibody (MACS, 130-091-024) and fixed with 2 % paraformaldehyde according to the manufacture's instructions. Thereafter, the T lymphocyte populations were investigated by a FACS analyzer (BD FACS Calibur, Becton Dickinson). The CD-25 positive T lymphocytes were considered as activated.

Statistical Analysis

Statistical variations were tested by applying the Wilcoxon rank-sum Test (p values ≤ 0.05 were regarded as statistically different). Data are reported as means $\pm$ standard deviation ($n = 3$).

Results and Discussion

Equalizing Gravitation Through Random Positioning

The basic idea followed, to generate simulated microgravity, is to distribute the Earth's gravity vector in space evenly over time by constantly reorienting the sample chamber to random positions (van Loon 2007). Therefore the RPM can be treated as a quasi-static machine (if the time frames are chosen small enough). Kinematic effects greatly depend on the position of the sample and the rotation velocity. Since the rotation velocity is small, kinematic effect such as centrifugal forces are negligible. In this section the concept of quasi-static random positioning is discussed in more details.

Gravity Vector Transposition to the Inner Frame

For the examination, it is important to distinguish between the static global and the rotating local frame (coordinate system) of the inner frame (Figs. 1 and 2). The moving frames of the RPM are mounted in the global frame, which is fixed, and gravity acts always normal to the ground (representing the global XY-plane). The local inner frame represents the frame (coordinate system) of the sample and is constantly reoriented with respect to the global frame. The gravity vector of the global frame is transposed into the local inner frame. This decomposition of the gravity vector to the inner coordinate system (where the samples are mounted) is computed, by employing two rotational matrixes. For this operation the position of the outer and inner frames needs to be known:

$$\vec{g}_I(t) = {}^{I}_{O}R(t) \cdot {}^{O}_{G}R(t) \cdot \vec{g}_G$$

$$\vec{g}_I(t) = \begin{bmatrix} \cos\beta(t) & 0 & \sin\beta(t) \\ 0 & 1 & 0 \\ -\sin\beta(t) & 0 & \cos\beta(t) \end{bmatrix} \cdot \begin{bmatrix} 1 & 0 & 0 \\ 0 & \cos\alpha(t) & -\sin\alpha(t) \\ 0 & \sin\alpha(t) & \cos\alpha(t) \end{bmatrix} \cdot \begin{pmatrix} 0 \\ 0 \\ -1 \end{pmatrix}$$

$$\vec{g}_I(t) = \begin{pmatrix} -\cos\alpha(t) \cdot \sin\beta(t) \\ \sin\alpha(t) \\ -\cos\alpha(t) \cdot \cos\beta(t) \end{pmatrix}$$

Random Walk

To equalize gravity we employ a Random Walk algorithm by which both frames of the RPM rotate at a constant velocity, but the rotation direction is inverted at randomly chosen time points. The velocity transition from forward to backward rotation takes place at a constant rotational acceleration.

Plotting the local gravity vector of the inner frames over the course of time, it becomes clear that the vector tip travels on a sphere with a radius of 1 g. However the distribution is not entirely even and concentrates at the two poles lying at the rotational axis of the inner frame (local Y-axis; Fig. 3). They become predominant after a short time. This phenomenon can be explained by the rotation of the outer frame. Every time the outer frame is in a vertical position, with the rotation axis of the inner frame parallel to the gravity, the local gravity vector is unavoidably pulled towards one of the two poles. In general, the resulting picture is symmetrical. Figure 4 illustrates the time course of how many times the Earth's gravity vector is pointing to an arbitrary position after a given period of time (1, 6, 15, 30, 60 min and 5 h).

Mean Gravity

As a quality measure for the distribution of orientation, we use the mean gravity over time, defined as:

$$G_{mean} = \sqrt{\left(G_{X,mean}\right)^2 + \left(G_{Y,mean}\right)^2 + \left(G_{Z,mean}\right)^2}$$

where the mean gravity values in the three directions are defined as follows:

$$G_{X,mean} = \frac{\sum_{i=1}^{n} g_{X,I,i}}{n}$$

$$G_{Y,mean} = \frac{\sum_{i=1}^{n} g_{Y,I,i}}{n}$$

$$G_{Z,mean} = \frac{\sum_{i=1}^{n} g_{Z,I,i}}{n}$$

The mean gravity is easy to compute and memory efficient, since only the sum of all samples in X, Y and Z, as well as the total number of samples, has to be stored. In Fig. 5 the mean gravity is plotted over time. The mean gravity falls quickly below 0.1 g and stabilizes below 0.03 g within 2 h of operation. With this concept two points lying opposite each other (sign change) are compensated. Therefore the two poles seen in Fig. 4 also cancel themselves out. In Fig. 5

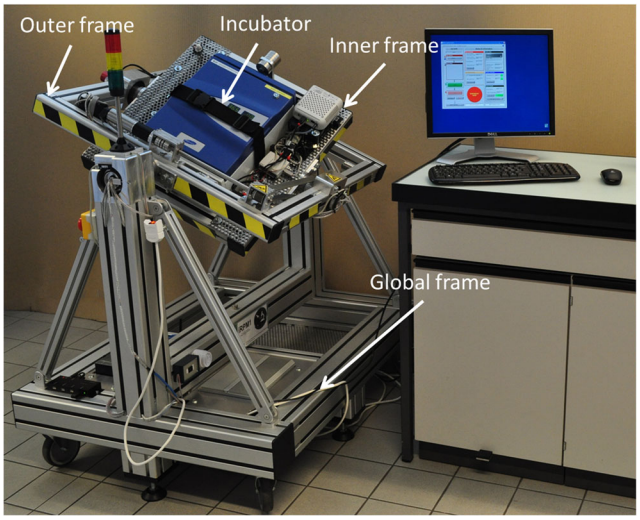

Fig. 1 Picture of the RPM construction. A CO_2 incubator is mounted in the center of the gimbal framework. The frames are driven by two independent precision motors

a temporal increase between approximately 0.5 and 1.5 h is visible. This appears because the Random Walk algorithm is based on random numbers and because the mean gravity is computed through averaging. At the beginning of an experiment little data contribute to the average, making it sensitive to any deviations. With the elapsing experiment time, the mean gravity becomes increasingly robust. This temporal increase of the mean gravity thus depends on the combination of the random numbers.

Numerical Illustration

Since the Random Walk algorithm depends on random numbers, the outcome of two successive runs, are not identical. To demonstrate the reliability of the algorithm several hundred runs of numerical simulations were performed. Each of these simulations represents an experiment of several hours. The resulting mean gravity at a defined time were finally recorded and plotted as a histogram. As shown in Fig. 6, all values stay below 0.03 g. The mean value of these 500 samples is 0.0086 g ± 0.0039 g (SD) for a rotational velocity of 60 deg/sec and 0.0105 g ± 0.0044 g (SD) for 40 deg/sec. The histograms in Fig. 6 are illustrating that the Random Walk is reliably producing simulated microgravity at both velocities. For particular angular velocities and assuming piecewise constant accelerations, it is possible to show that the expected mean squared gravity vanishes over time. The approach, based on a central limit theorem, is mathematically quite involved and is outside the scope of this article.

Kinematics

For slow rotations the quasi-static approach is sufficiently valid and applies for all samples close enough to the center of rotation. The acceleration caused by kinematics is, however, much more difficult to deal with and depends greatly on the sample position relative to the center of rotation (Fig. 7).

The experienced acceleration of an arbitrary point can be computed as follows: Any point $\overrightarrow{p}_{local}$ in the inner frame can be described with a vector $\overrightarrow{r}_{local}$ from the center of rotation. The path of $\overrightarrow{p}_{local}$ in the global frame, as both frames rotate, is computed by employing two rotational matrixes:

$$\overrightarrow{p}_{global} = {}^{G}_{O}R \cdot {}^{O}_{I}R \cdot \overrightarrow{r}_{local}$$

$$\overrightarrow{p}_{global}(t) = \begin{bmatrix} 1 & 0 & 0 \\ 0 & \cos(\omega_\alpha \cdot t + \alpha_0) & \sin(\omega_\alpha \cdot t + \alpha_0) \\ 0 & -\sin(\omega_\alpha \cdot t + \alpha_0) & \cos(\omega_\alpha \cdot t + \alpha_0) \end{bmatrix} \cdot \begin{bmatrix} \cos(\omega_\beta \cdot t + \beta_0) & 0 & -\sin(\omega_\beta \cdot t + \beta_0) \\ 0 & 1 & 0 \\ \sin(\omega_\beta \cdot t + \beta_0) & 0 & \cos(\omega_\beta \cdot t + \beta_0) \end{bmatrix} \cdot \begin{bmatrix} r_{X,local} \\ r_{Y,local} \\ r_{Z,local} \end{bmatrix}$$

By differentiating the position twice with respect to time we get the accelerations $A_{X,global}(t)$, $A_{Y,global}(t)$ and $A_{Z,global}(t)$, acting in the direction of the global coordinate systems axis X, Y and Z, respectively. From these three accelerations the absolute acceleration magnitude A_{global} can be computed.

$$A_{global}(t) = \sqrt{\left[A_{X,global}(t)\right]^2 + \left[A_{Y,global}(t)\right]^2 + \left[A_{Z,global}(t)\right]^2}$$

To simplify, we assume that both frames rotate with an identical velocity, $\omega_\alpha = \omega_\beta = \omega$. The terms α_0 and β_0 can

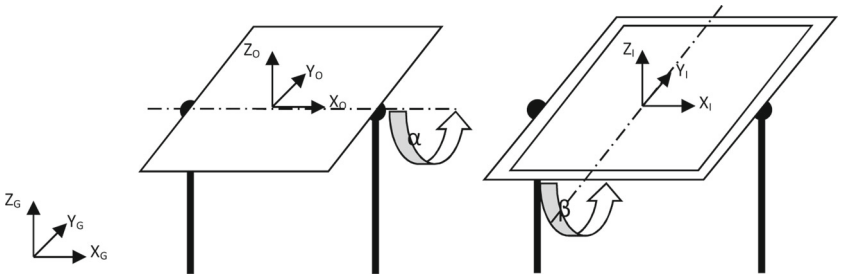

Fig. 2 Schematic of the RPMs gimbal framework. The samples (on the inner frame) are rotated around two perpendicular axes

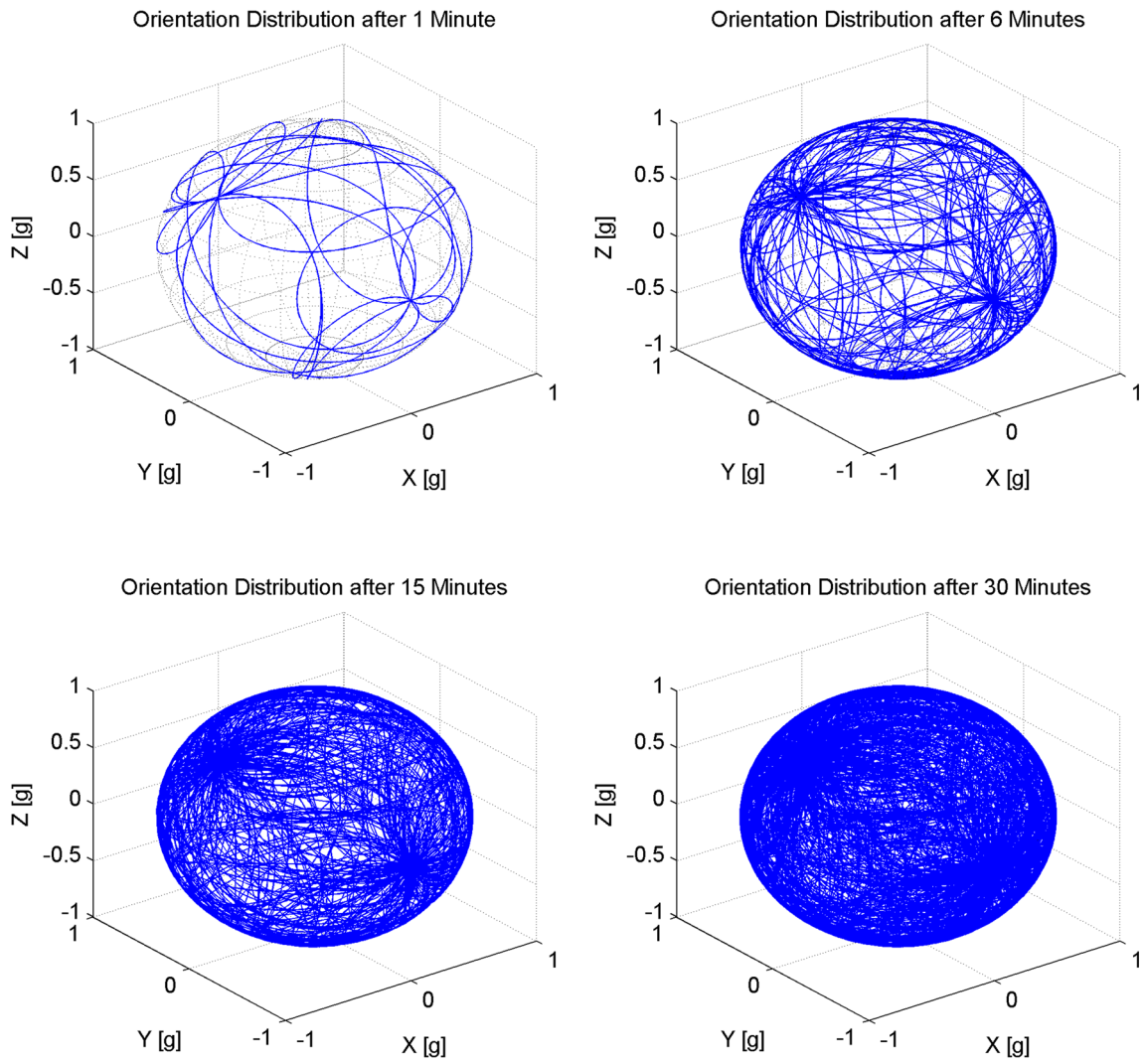

Fig. 3 Distribution of the local gravity vector over the course of time. The *blue line* indicates the path of the gravity vector, as it would be experienced by a sample at the center of rotation. The local gravity vector frequently passes through two poles lying on the *Y*-axis (rotation axis of inner frame). This becomes clearly visible already after 6 min (*top left*). (Random Walk, Velocity: 60 deg/sec)

be set to zero ($\alpha_0 = \beta_0 = 0$), since they have no influence on the mean and peak acceleration. This results in:

$$A_{global}(t) = \omega^2 \cdot \sqrt{\left(r_{X,local}^2\left(4.5 + \frac{\cos(2\cdot\omega\cdot t)}{2}\right)\right.}$$
$$+ r_{Y,local}^2 + r_{Z,local}^2\left(4.5 - \frac{\cos(2\cdot\omega\cdot t)}{2}\right)$$
$$- r_{X,local}\cdot r_{Y,local}\cdot 4\cdot\cos(\omega\cdot t) - r_{X,local}\cdot r_{Z,local}$$
$$\left.\cdot\sin(2\cdot\omega\cdot t) + r_{Y,local}\cdot r_{Z,local}\cdot 4\cdot\sin(\omega\cdot t)\right)$$

From this formula we can approximate the mean acceleration:

$$A_{mean,global} \approx \omega^2\sqrt{4.5\cdot r_{X,local}^2 + r_{Y,local}^2 + 4.5\cdot r_{Z,local}^2}$$

To illustrate the formula above, path and total acceleration for three different points are shown in Fig. 7. All points have the same radius length but acceleration is by far not the same.

$$\vec{r}_1 = \frac{0.1\,[\mathrm{m}]}{\sqrt{3}}\begin{pmatrix}1\\1\\1\end{pmatrix} \qquad \vec{r}_2 = \frac{0.1\,[\mathrm{m}]}{\sqrt{2}}\begin{pmatrix}1\\0\\1\end{pmatrix}$$

$$\vec{r}_3 = 0.1\,[\mathrm{m}]\begin{pmatrix}0\\1\\0\end{pmatrix}$$

Even though the kinematic acceleration depends on the location, it is limited to a range given by the rotation velocity and the distance from the center of rotation:

$$\breve{A}_{mean,global} \approx \omega^2 \cdot r$$

$$\hat{A}_{mean,global} \approx \frac{3}{\sqrt{2}}\cdot\omega^2\cdot r$$

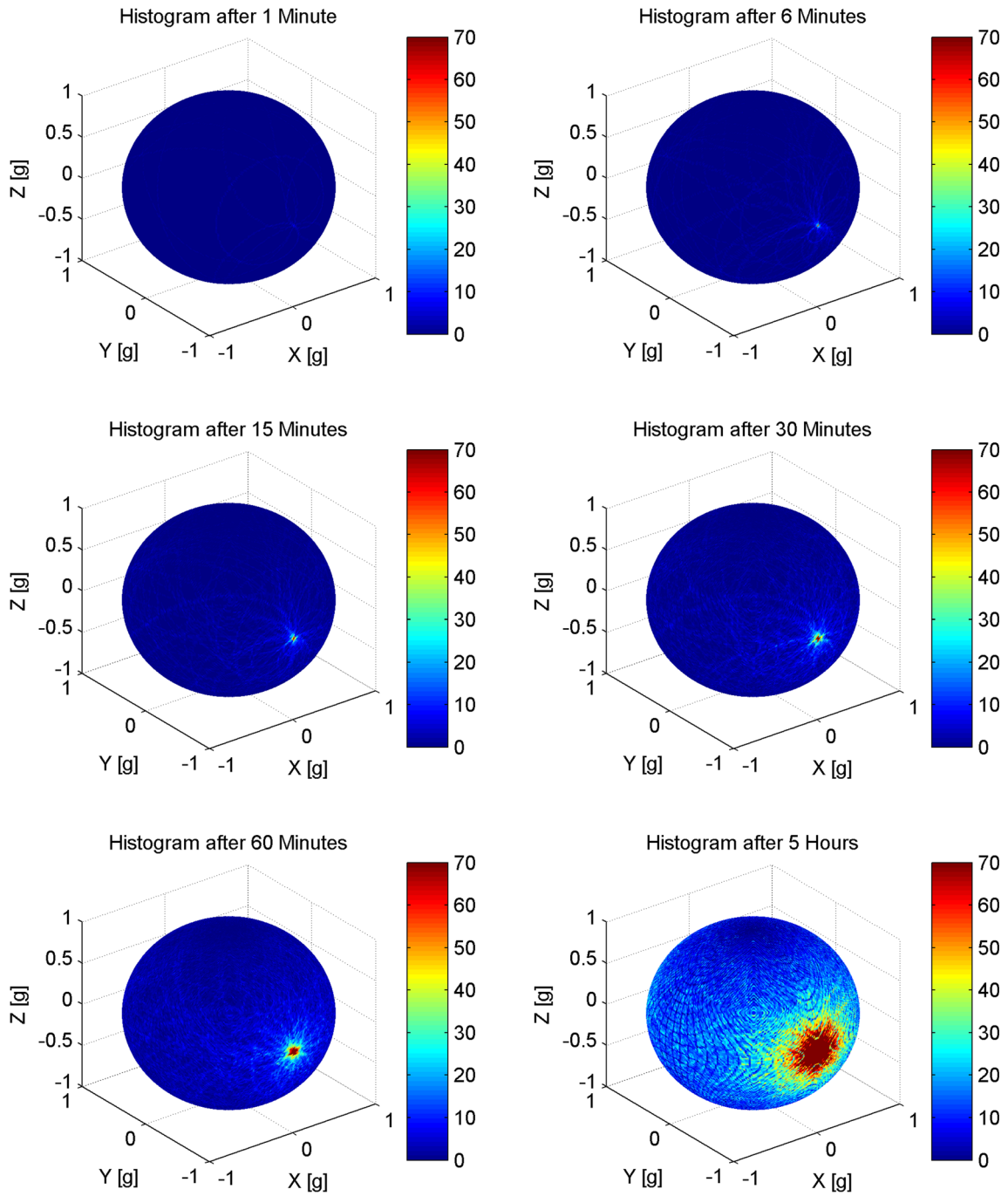

Fig. 4 Histograms of the orientation mapped as color code on an imaginary sphere. The color of a particular spot on the sphere indicates how often the gravity vector pointed at that direction. According to the simulation, the orientation distribution is uneven, but symmetrical and two poles become dominant after a short time (Random Walk, Velocity: 60 deg/sec, $f_s = 50$ Hz)

Local Acceleration

The acceleration computed in the global frame (for a specific time point) is not the acceleration experienced by a point in the local frame. To be more precise, the absolute value of the local and global acceleration is the same, but not the direction:

$$\left|\overrightarrow{A}_{global}(t)\right| = \left|\overrightarrow{A}_{local}(t)\right| \qquad \overrightarrow{A}_{global}(t) \neq \overrightarrow{A}_{local}(t)$$

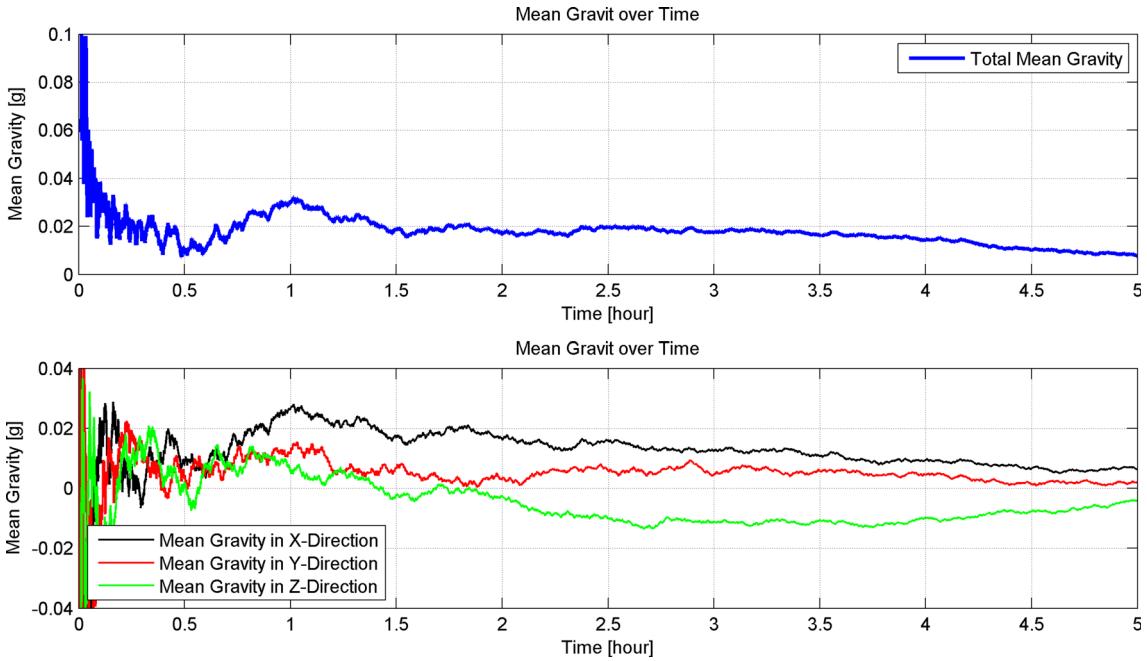

Fig. 5 The mean gravity (*upper track*) as well as the mean gravity of the components in the *X*-, *Y*- and *Z*- directions (*lower track*) plotted over time. The temporal increase between 0.5 and 1.5 h appear because the Random Walk algorithm is based on random numbers and because the mean gravity is computed through averaging. With the elapsing experiment time, the mean gravity becomes increasingly robust to temporal deviations

To compute the local acceleration the global acceleration has to be transformed by again employing the above rotation matrixes:

$$\vec{A}_{local}(t) = {}^{0}_{I}R^{T} \cdot {}^{G}_{0}R^{T} \cdot \vec{A}_{global}(t)$$

$$\vec{A}_{local}(t) = \begin{bmatrix} \cos(\omega_\beta \cdot t + \beta_0) & 0 & \sin(\omega_\beta \cdot t + \beta_0) \\ 0 & 1 & 0 \\ -\sin(\omega_\beta \cdot t + \beta_0) & 0 & \cos(\omega_\beta \cdot t + \beta_0) \end{bmatrix} \cdot \begin{bmatrix} 1 & 0 & 0 \\ 0 & \cos(\omega_\alpha \cdot t + \alpha_0) & -\sin(\omega_\alpha \cdot t + \alpha_0) \\ 0 & \sin(\omega_\alpha \cdot t + \alpha_0) & \cos(\omega_\alpha \cdot t + \alpha_0) \end{bmatrix} \cdot \vec{A}_{global}(t)$$

Again we can set the terms α_0 and β_0 to zero ($\alpha_0 = \beta_0 = 0$). The rotation velocity shall be the same for both frames, $\omega_\alpha = \omega_\beta = \omega$. After substituting and simplifying we finally get:

$$\vec{A}_{local}(t) = \omega^2 \begin{pmatrix} r_{X,local} \cdot \frac{\cos(2\cdot\omega\cdot t)-3}{2} - r_{Z,local} \cdot \frac{\sin(2\cdot\omega\cdot t)}{2} \\ r_{X,local} \cdot 2 \cdot \cos(\omega \cdot t) - r_{Y,local} - r_{Z,local} \cdot 2 \cdot \sin(\omega \cdot t) \\ -r_{X,local} \cdot \frac{\sin(2\cdot\omega\cdot t)}{2} - r_{Z,local} \cdot \frac{\cos(2\cdot\omega\cdot t)+3}{2} \end{pmatrix}$$

By computing the mean gravity, we first compute the mean gravity for all three components in *X*, *Y* and *Z* and then we

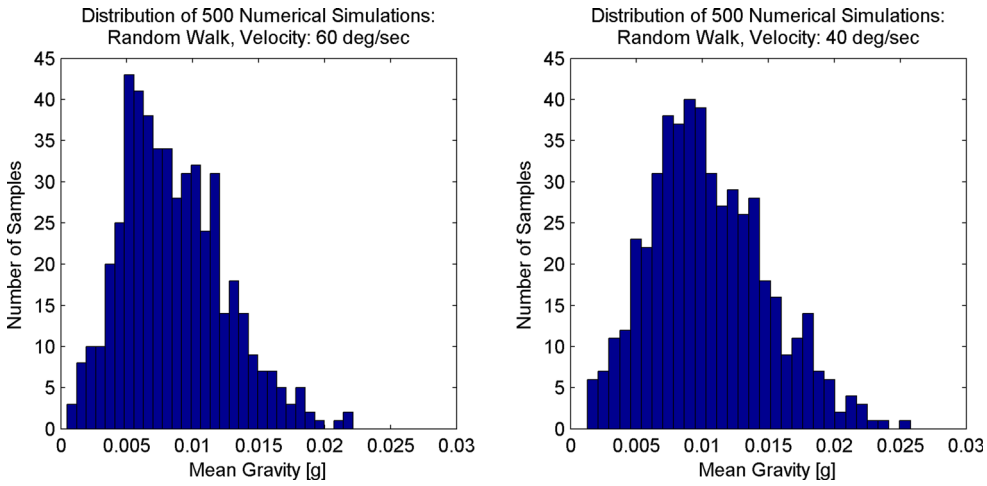

Fig. 6 Histograms of 500 numerical simulations. Each sample represents the mean gravity at the center of rotation after 5 h in operation. *Left:* Random Walk, velocity: 60 deg/sec. *Right:* Random Walk, velocity 40 deg/sec. The histograms are illustrating that the Random Walk is reliably producing simulated microgravity at both velocities

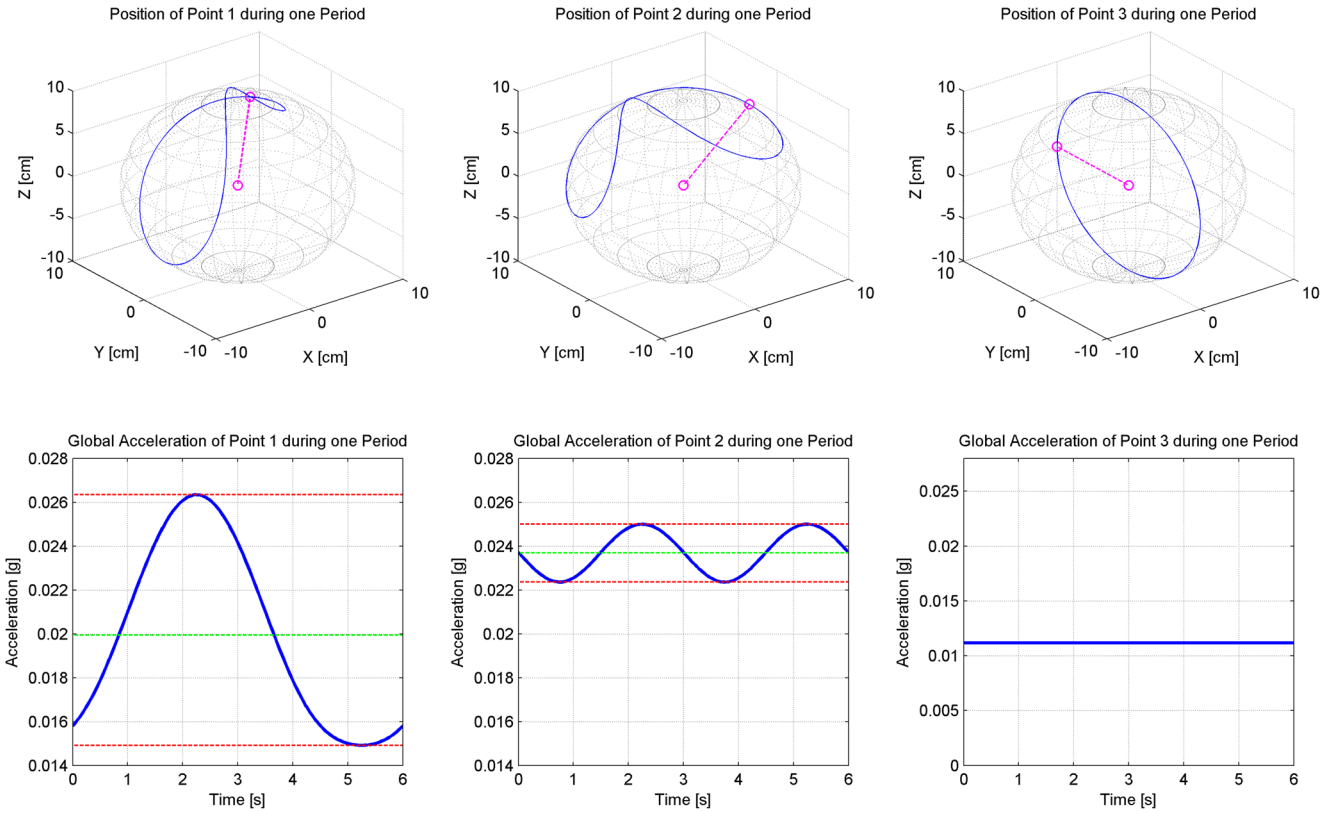

Fig. 7 Path and acceleration for three points with the same distance from the center of rotation. Both (outer and inner) frames rotate at a constant velocity with 60 deg/sec. The *top row* shows the path in *blue*. The vector in *magenta* indicates the position of the specific point at time $t = 0$. On the *bottom row*, the global acceleration as a function of time (*in blue*) and the corresponding mean (*green*) as well as the minimum and maximum (*red*) is plotted. The resulting accelerations depend greatly on the position, even though the distance to the center of rotation is the same

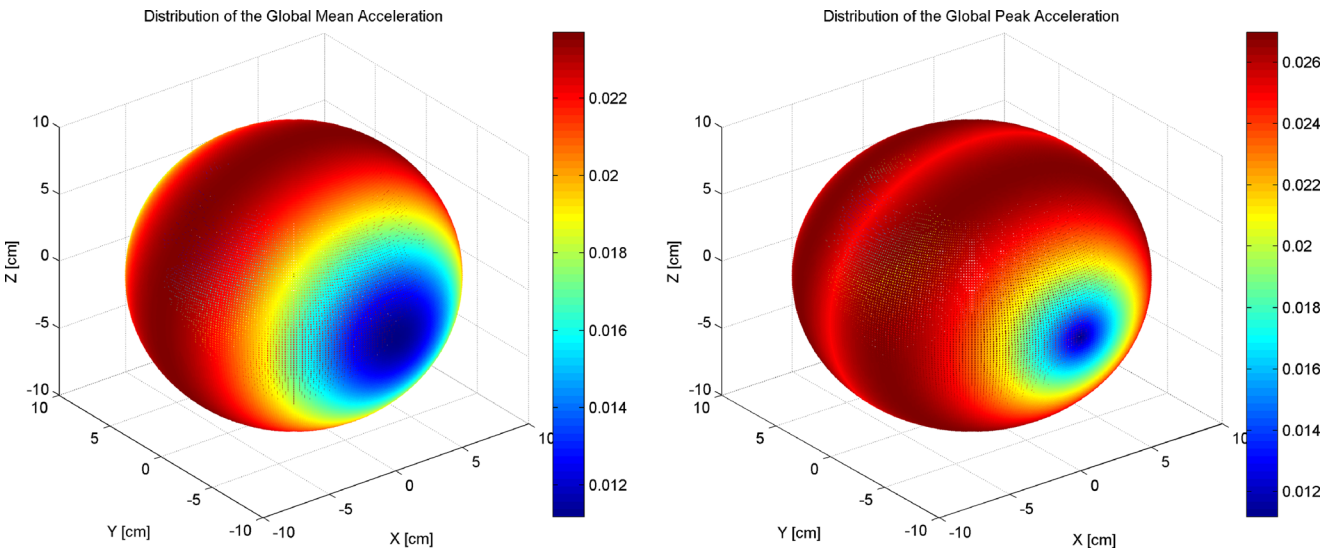

Fig. 8 The mean global acceleration ($A_{mean,global}$) and peak global acceleration ($\hat{A}_{global}$) depending on the location ($r = 10$ cm; $\omega = 60$ deg/sec)

compute the total mean gravity by using the vector addition. If we do the same for the local acceleration we get:

$$\vec{A}_{mean,local} = \omega^2 \begin{pmatrix} -1.5 \cdot r_{X,local} \\ -r_{Y,local} \\ -1.5 \cdot r_{Z,local} \end{pmatrix}$$

$$A_{mean,local} = \left| \vec{A}_{mean,local} \right| = \omega^2 \sqrt{2.25 \cdot r_{X,local}^2 + r_{Y,local}^2 + 2.25 \cdot r_{Z,local}^2}$$

Acceleration Depending on the Position

As we have already seen above, the experienced acceleration of a point depends strongly on the location. By iterating through multiple points on a sphere and computing the mean global acceleration ($A_{mean,global}$) and the peak acceleration ($\hat{A}_{global}$), we get the results illustrated in Fig. 8. The radius length r is constant and set to 10 cm. By visualizing the peak acceleration, it becomes clear that the highest peak accelerations do not appear at the same locations as the highest mean accelerations (Fig. 8). The points on the *XZ*-plane (being perpendicular to the rotation axis of the inner frame) experience the highest mean acceleration. The highest peak accelerations appear on two planes parallel to the *XZ*-plane and are approximately $0.38 \cdot r$ away from the *XZ*-plane. The smallest accelerations appear on the two points lying on the rotation axis of the inner frame (*Y*-axis).

Experimental Validation

T Lymphocytes purified from human peripheral blood can be activated by Con A *in vitro*. The drug, a lectin extracted from lentil seeds, exerts this effect by mimicking the antigen-presenting process occurring during specific antigen-activation. The transmembrane protein CD25, which is highly expressed on the surface of activated T lymphocytes, is used as a marker for the activation. Several experiments have already shown that T lymphocytes reduce their activation substantially on exposure to reduced gravity (either during space flights, sounding rocket or RPM)(Cogoli-Greuter et al. 1994; Cogoli et al. 1984). We use this effect to validate the quality of the algorithm running on the novel RPM that generates simulated microgravity for samples in the center of the rotating frames. By comparing the activation values of samples under normal 1 g conditions, simulated microgravity (created by the old and established RPM as well as by the novel RPM), as well as real space conditions, it appears that the simulated reduction of the gravity field leads to a reduction of the T lymphocytes activation by about 80–90 % (Fig. 9). These results are in agreement with previous publications (Cogoli et al. 1984; Gmunder et al. 1990; Cogoli-Greuter et al. 1994).

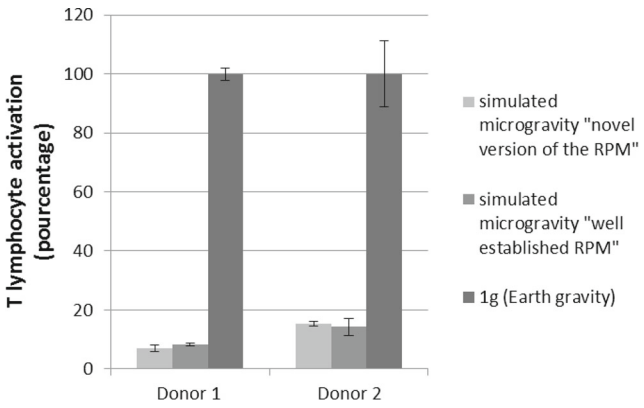

Fig. 9 T lymphocyte activation by Con A/CD28 under 1 g and simulated microgravity. Two healthy donors were tested

Conclusions

Here, we present a novel version of a RPM that is applicable for experiments in the field of life science concerning microgravity and 3D cell culturing. Our new machine applies the well-established core principle of gravity nullification, a concept that was introduced decades ago (van Loon 2007; Borst and Van Loon 2009). In this novel RPM includes features like stable environmental conditions (temperature, CO_2 etc.) in the culture chamber as well as a constant supply of culture media or CO_2 to the samples, which creates much better long-term cell culturing conditions than before.

A major objective of the novel RPM is to simulate microgravity as accurately as possible. Thus, a major effort was put into the theoretical concept of gravity nullification as well as the conversion of that concept into the algorithm controlling the movement of the frames. As we have shown here, by applying the newly designed algorithm, the mean gravity falls below 0.1 g within a few minutes and stabilizes below 0.03 g thereafter within 2 h. The mathematical analysis further demonstrated that samples placed anywhere in the incubator experience low gravity levels. Despite the difficulty to completely control kinematic accelerations, they are limited to a given range, only depending on the rotation velocity and the samples' distance from the center of rotation. These two parameters should therefore be kept as low as possible. This novel RPM represents a valid tool for simulating microgravity. This was confirmed by conducting experiments with human T lymphocytes. Their behavior under microgravity (simulated on real space microgravity) is well known and has been described in numerous publications (Cogoli et al. 1984; Cogoli-Greuter et al. 1994; Gmunder et al. 1990). As illustrated in Fig. 9, exposing T lymphocytes to reduced gravity leads to a severe reduction of the activation. The figure further elucidates that there is

no difference between the old and well-established RPM and our novel version of the RPM (Fig. 9). This indicates that the algorithm of the novel RPM is comparable to the one of the old RPM.

However, the novel version of the RPM is not only an interesting tool for microgravity-related biological studies. Long-term cultivation of cells under low gravity conditions offers new aspects for tissue engineering. By adding the described features, long-term cultivation of cells under simulated microgravity is now possible for the first time and is of a comparable quality to regular (stationary) cell cultures. Permanent exchange of culture media can be precisely controlled by the novel RPM, as well as the addition of particular drugs to the cell cultures at a particular time of day for a defined period of time. Built in log files record any action of the system allowing a retrospective analysis of the experiment. Our former studies have already demonstrated that long-term cultivation of endothelial cells under simulated microgravity conditions leads to spheroidal growth behavior, including vascularization (Pietsch et al. 2011). Thus, this novel version of the RPM offers an ideal platform for studies such as tumor growth.

It will be interesting in future studies to show how other cell types respond to cultivation under reduced gravity or under mechanical unloading. It is likely that this culture method bears new options and possibilities for cell culturing in general, allowing tissue to grow that shows unexpected features.

References

Anders, M., Hansen, R., Ding, R.X., Rauen, K.A., Bissell, M.J., Korn, W.M.: Disruption of 3D tissue integrity facilitates adenovirus infection by deregulating the coxsackievirus and adenovirus receptor. Proc. Natl. Acad. Sci. U. S. A. **100**(4), 1943–1948 (2003)

Barrila, J., Radtke, A.L., Crabbe, A., Sarker, S.F., Herbst-Kralovetz, M.M., Ott, C.M., Nickerson, C.A.: Organotypic 3D cell culture models: using the rotating wall vessel to study host-pathogen interactions. Nat. Rev. Microbiol. **8**(11), 791–801 (2010)

Borst, A.G., Van Loon, J.J.: Technology and Developments of the Random Positioning Machine. RPM. Microgravity Sci. Technol. **21**, 287–292 (2009)

Butcher, J.T., Nerem, R.M.: Porcine aortic valve interstitial cells in three-dimensional culture: comparison of phenotype with aortic smooth muscle cells. J. Heart Valve Dis. **13**(3), 478–485 (2004). discussion 485–476

Cadee, J.A., van Luyn, M.J., Brouwer, L.A., Plantinga, J.A., van Wachem, P.B., de Groot, C.J., den Otter, W., Hennink, W.E.: In vivo biocompatibility of dextran-based hydrogels. J. Biomed. Mater. Res. **50**(3), 397–404 (2000)

Cascone, M.G., Barbani, N., Cristallini, C., Giusti, P., Ciardelli, G., Lazzeri, L.: Bioartificial polymeric materials based on polysaccharides. J. Biomater. Sci. Polym. Ed. **12**(3) (2001)

Chang, T.T., Walther, I., Li, C.F., Boonyaratanakornkit, J., Galleri, G., Meloni, M.A., Pippia, P., Cogoli, A., Hughes-Fulford, M.: The Rel/NF-kappaB pathway and transcription of immediate early genes in T cell activation are inhibited by microgravity. J. Leukoc. Biol. **92**(6), 1133–1145 (2012)

Cogoli, A., Tschopp, A., Fuchs-Bislin, P.: Cell sensitivity to gravity. Sci. **225**(4658), 228–230 (1984)

Cogoli-Greuter, M., Pippia, P., Sciola, L., Cogoli, A.: Lymphocytes on sounding rocket flights. J. Gravit. Physiol. **1**(1), P90—91 (1994)

Cogoli-Greuter, M., Meloni, M.A., Sciola, L., Spano, A., Pippia, P., Monaco, G., Cogoli, A.: Movements and interactions of leukocytes in microgravity. J. Biotechnol. **47**(2–3), 279–287 (1996)

Eyrich, D., Brandl, F., Appel, B., Wiese, H., Maier, G., Wenzel, M., Staudenmaier, R., Goepferich, A., Blunk, T.: Long-term stable fibrin gels for cartilage engineering. Biomater. **28**(1), 55–65 (2007)

Friedrich, J., Seidel, C., Ebner, R., Kunz-Schughart, L.A.: Spheroid-based drug screen: considerations and practical approach. Nat. Protoc. **4**(3), 309–324 (2009)

Gmunder, F.K., Kiess, M., Sonnefeld, G., Lee, J., Cogoli, A.: A ground-based model to study the effects of weightlessness on lymphocytes. Biol. Cell **70**(1–2), 33–38 (1990)

Ho, S.T., Cool, S.M., Hui, J.H., Hutmacher, D.W.: The influence of fibrin based hydrogels on the chondrogenic differentiation of human bone marrow stromal cells. Biomater. **31**(1), 38–47 (2010)

Hughes, C.S., Postovit, L.M., Lajoie, G.A.: Matrigel: a complex protein mixture required for optimal growth of cell culture. Proteomics **10**(9), 1886–1890 (2010)

Ivascu, A., Kubbies, M.: Rapid generation of single-tumor spheroids for high-throughput cell function and toxicity analysis. J. Biomol. Screen. **11**(8), 922–932 (2006)

Kleinman, H.K., McGarvey, M.L., Liotta, L.A., Robey, P.G., Tryggvason, K., Martin, G.R.: Isolation and characterization of type IV procollagen, laminin, and heparan sulfate proteoglycan from the EHS sarcoma. Biochem. **21**(24), 6188–6193 (1982)

Kleinman, H.K., McGarvey, M.L., Hassell, J.R., Star, V.L., Cannon, F.B., Laurie, G.W., Martin, G.R.: Basement membrane complexes with biological activity. Biochem. **25**(2), 312–318 (1986)

Kraft, T.F., van Loon, J.J., Kiss, J.Z.: Plastid position in Arabidopsis columella cells is similar in microgravity and on a random-positioning machine. Planta **211**(3), 415–422 (2000)

Lin, R.Z., Chang, H.Y.: Recent advances in three-dimensional multicellular spheroid culture for biomedical research. Biotechnol. J. **3**(9–10), 1172–1184 (2008)

Masters, K.S., Shah, D.N., Leinwand, L.A., Anseth, K.S.: Crosslinked hyaluronan scaffolds as a biologically active carrier for valvular interstitial cells. Biomater. **26**(15), 2517–2525 (2005)

Pietsch, J., Sickmann, A., Weber, G., Bauer, J., Egli, M., Wildgruber, R., Infanger, M., Grimm, D.: A proteomic approach to analysing spheroid formation of two human thyroid cell lines cultured on a random positioning machine. Proteomics **11**(10), 2095–2104 (2011)

Pippia, P., Sciola, L., Cogoli-Greuter, M., Meloni, M.A., Spano, A., Cogoli, A.: Activation signals of T lymphocytes in microgravity. J. Biotechnol. **47**(2–3), 215–222 (1996)

Santini, M.T., Rainaldi, G.: Three-dimensional spheroid model in tumor biology. Pathobiology **67**(3), 148–157 (1999)

Shaw, K.R., Wrobel, C.N., Brugge, J.S.: Use of three-dimensional basement membrane cultures to model oncogene-induced changes in mammary epithelial morphogenesis. J. Mammary Gland Biol. Neoplasia **9**(4), 297–310 (2004)

van Loon, J.J.: Some history and use of the random positioning machine, RPM, in gravity related research. Adv. Space Res. **39**, 1161–1165 (2007)

Weaver, V.M., Petersen, O.W., Wang, F., Larabell, C.A., Briand, P., Damsky, C., Bissell, M.J.: Reversion of the malignant phenotype

of human breast cells in three-dimensional culture and in vivo by integrin blocking antibodies. J. Cell Biol. **137**(1), 231–245 (1997)

Wenger, A., Stahl, A., Weber, H., Finkenzeller, G., Augustin, H.G., Stark, G.B., Kneser, U.: Modulation of In Vitro Angiogenesis in a Three-Dimensional Spheroidal Coculture Model for Bone Tissue Engineering. Tissue Eng. **10**(9–10), 1536–1547 (2004)

Wenger, A., Kowalewski, N., Stahl, A., Mehlhorn, A.T., Schmal, H., Stark, G.B., Finkenzeller, G.: Development and Characterization of a Spheroidal Coculture Model of Endothelial Cells and Fibroblasts for Improving Angiogenesis in Tissue Engineering. Cells Tissues Organs **181**(2), 80–88 (2005)

Wolf, K., Mazo, I., Leung, H., Engelke, K., von Andrian, U.H., Deryugina, E.I., Strongin, A.Y., Brocker, E.B., Friedl, P.: Compensation mechanism in tumor cell migration: mesenchymal-amoeboid transition after blocking of pericellular proteolysis. J. Cell Biol. **160**(2), 267–277 (2003)

Burdick, J.A., Prestwich, G.D.: Hyaluronic acid hydrogels for biomedical applications. Adv. Mater. **23**(12), H41–56 (2011). doi:10.1002/adma.201003963